THE ASTROPHYSICAL JOURNAL, 280:428–439, 1984 May 1

CORONAL TRANSIENT GEOMETRY. I. THE FLARE-ASSOCIATED EVENT OF 1981 MARCH 25

RICHARD R. FISHER AND RICHARD H. MUNRO
High Altitude Observatory, National Center for Atmospheric Research[1]
Received 1983 April 21; accepted 1983 October 18

ABSTRACT

On 1981 March 25 a large white light coronal transient, associated with an optical 2B flare and X 2.2 X-ray event, was observed over the west limb of the Sun with the Mk III *K*-coronameter. This event, although one of the first described in the lower corona, 1.2 $R_\odot$ to 2.4 $R_\odot$, is typical of flare-associated coronal transients seen at higher altitudes. The apparent speed of the leading edge of the structure ranged from 556 to 800 km s^{-1}. The estimated mass of the material injected into the field of view above the occulting disk is $2.0 \times 10^{+15}$ g. Postevent observations indicate that not only did this material leave the field of view of the instrument, but that preexisting coronal material was also depleted from the field of view—an amount estimated to be an additional $2.2 \times 10^{+15}$ g.

From the postevent depleted region, a lower limit for the *minimum* thickness of the event along the line of sight was estimated to be equal to 0.52 $R_\odot$ at a height of 1.5 $R_\odot$ (assuming a perfectly evacuated region). The observed distribution of polarized brightness, *pB*, is modeled by a simple, three-dimensional figure which has a symmetry axis perpendicular to the limb. A detailed comparison of inferred radial and azimuthal distributions of *pB* are compared to the observed quantities. This simple model is capable of reproducing the major features of the transient: the bright leading edge and legs as well as the depleted region behind the leading edge. The characteristics of the inferred changes in coronal mass from the model are consistent with those estimated from the observations.

Subject heading: Sun: flares

I. INTRODUCTION

A class 2B flare was observed near the west limb of the Sun beginning at 2038 UT (McCabe 1981) on 1981 March 25. Observation of the 1–8 Å X-ray flux by detectors on the *GOES 2* spacecraft indicate the beginning of an X 2.2 X-ray event at 2036 UT, an event characterized by a rapid increase in the flux and a slow decay lasting some 3 hours (*Solar Geophysical Data 1981*). Associated with this event the Culgoora spectrograph recorded both a type II burst beginning at 2042:45 UT, and later a stationary type IV burst (Stewart 1981). The imaging Mk III *K*-coronameter at the Mauna Loa Solar Observatory detected a large white light coronal transient which was closely associated in both time and space with optical, X-ray, and radio manifestations of activity.

The details of the *K*-coronameter and Hα observations are given elsewhere by Friend *et al.* (1982). The present work adds an analysis of the velocity properties of this particular transient, as well as a discussion of the density distribution and changes of coronal mass, to the previous study. A general goal of the present work is to address the questions of the morphology of this striking event and its density distribution along the line of sight. To accomplish this, a particular three-dimensional density distribution is postulated and then tested for its ability to reproduce the observable quantity, the polarized brightness of the lower corona.

A unique feature of this event which first attracted attention is shown in Figure 1. In the upper left-hand portion of this figure, a sample polarized brightness distribution is shown, as viewed with the real-time coronameter data system, about an hour prior to the occurrence of the transient. The post-transient state, at 2138 UT, is shown at the upper right; the difference between the two distributions is displayed below. This difference contour depicts relative depletions of the corona with solid lines; the convention of this real-time presentation is discussed in detail by Rock and Seagraves (1982). It is immediately obvious that a relatively large amount of mass has been removed from the lower corona in conjunction with the transient. A depletion may be used to set a lower limit to the dimension of the affected coronal volume along the line of sight. Such a limit is crucial in the determination of the geometry of the event.

The transient first appeared over the occulting disk during a scan at 2040 UT; at that time only a small bright mound was detected. In the next scan, started 94 s later, a small archlike feature is seen above the occulting disk. As the transient develops, the bright arch expands outward until leaving the field of view; the leading edge passed out of the field of view during the scan which began at 2058 UT. The Mk III *K*-coronameter has a field of view which extends from 1.18 $R_\odot$ to 2.38 $R_\odot$. The unvignetted field of view is restricted to a narrower height range of 1.24–2.18 $R_\odot$; however, the larger field of view is shown in Figure 2. The instrument uses a geocentric equatorial rectangular coordinate system; thus, a radius vector from the center of the Sun to the north point in the image is parallel to the rotational axis of the Earth; the fiducial marks on the two images refer to directions parallel and perpendicular to a radius drawn from Sun center. The images shown are ΔpB images; that is,

[1] The National Center for Atmospheric Research is sponsored by the National Science Foundation.

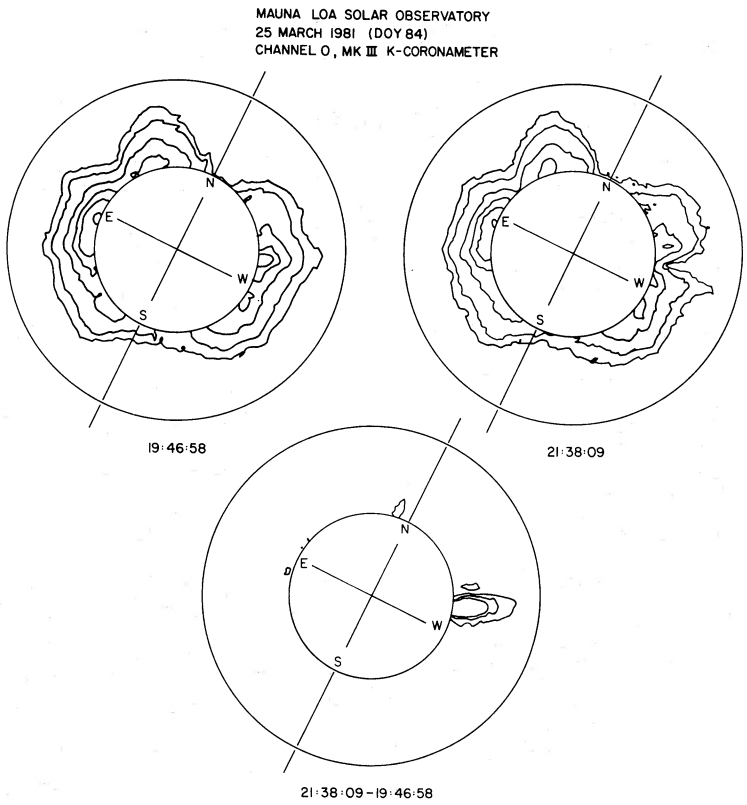

FIG. 1.—Real time and differenced coronal pB contour plots of the 1981 March 25 coronal transient. The depleted region is shown with solid lines; the contour intervals are $\Delta pB/pB = 0.1$, 0.2, and 0.3.

a base image taken at 2034 UT has been subtracted from the scan at the indicated times: 2055 and 2118 UT. At the time of the transient, the Mk III data system operated in a compressed data mode which retains a mean information density of 4.5 bits per pixel rather than the original 16 bits per pixel. As a result, the difference images appear slightly noisier than one would expect; occasional encounters of the sampling slit with airborne debris or insects account for the radially oriented image defects. In the ΔpB images, previously discussed by Fisher and Poland (1981), regions of the corona which are common to both the base and object images are shown with a zero level assigned to a background gray tone in the ΔpB image. Relatively enhanced or depleted regions of coronal density are then detected as lighter or darker areas of the image, respectively. Superposed on these two images are marks used to indicate the coordinate system and integration limits for the discussion of the geometry and mass properties.

In the upper image of Figure 2, the difference between the pB distribution (detected at 2055 and 2034 UT) shows the bright archlike structure just before the leading edge left the Mk III field of view. Two other features can be distinguished: these are the radially oriented legs of the transient, and a severely depleted volume, near the axis of symmetry, beneath the bright ring. The supposed axis of symmetry is marked with a radial line which is intersected with height marks. The azimuth of the radial axis is taken to be 264°; since the P-angle for 1981 March 25 was $-25\overset{\circ}{.}8$, the projected latitude for the source is 20° N. In the lower, post-transient image, the large depleted region first seen in the real-time data of Figure 1 is most obvious, as are the transient legs. Sectors of 10° and 70° were used to study the rate of change of inferred coronal mass as a function of radius. The placement of the wide (70°) and narrow (10°) sectors is shown on this later ΔpB image.

a) Kinematic and Photometric Properties

Radial scans of ΔpB at the geocentric azimuth of $\Theta_G = 264°$ for various times characterize the motion of the leading edge of the loop, the position of the peak polarization brightness in the loop, and the depleted region behind the leading edge. These radial scans, ΔpB as a function of h, are shown in Figure 3. The earliest is plotted at the top; subsequent traces are separated by 188 s. The zero level for each trace is indicated at the left and right, and a pB scale marker is given at the right for each scan time. Note that the scale changes by a factor of 2.5 between the first and second traces. As is commonly found in ΔpB images taken in the compressed data mode (4.5 bits per pixel), the peak to peak noise has an amplitude of about $1.2 \times 10^{-8}\ B_\odot$.

The position of the leading edge of the transient was taken to be the highest height at which the ΔpB trace departed significantly from zero. The position of the brightest part of the loop was taken to be the largest estimate of $\Delta pB(h)$ found to the left of the leading edge. From these two height definitions, it is possible to tabulate a height-versus-time

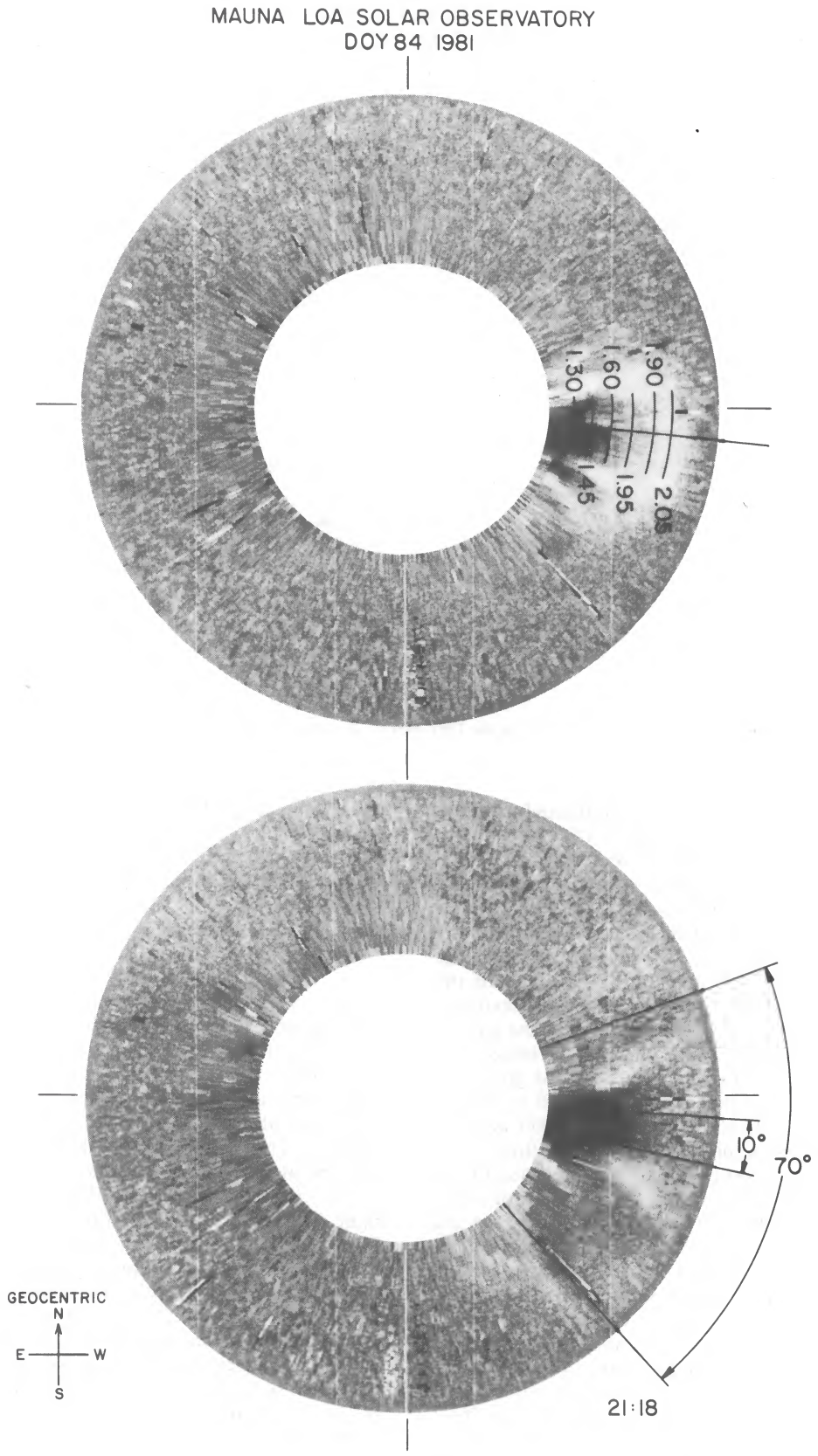

FIG. 2.—The coronal transient ΔpB images formed by subtracting the image from 2037 UT from the images obtained at 2056 and 2118 UT

TABLE 1

APPARENT SPEED OF ΔpB_{max}, AND LEADING EDGE

Time of Scan Start (UT)	Height of ΔpB_{max} ($h = R/R_\odot$)	ΔpB_{max} × 10^{-8} $B_\odot$	Apparent Speed of ΔpB_{max} (km s^{-1})	Height of Leading Edge ($h = R/R_\odot$)	Apparent Speed of Leading Edge (km s^{-1})
2043.....	1.25	12.3		...	
			556 ± 125		...
2046.....	1.41	12.3		1.61	
			626 ± 125		626 ± 175
2049.....	1.59	6.9		1.79	
			765 ± 125		800 ± 250
2052.....	1.81	4.2		2.02	
			730 ± 125		696 ± 270
2055.....	2.02	3.1		2.22	

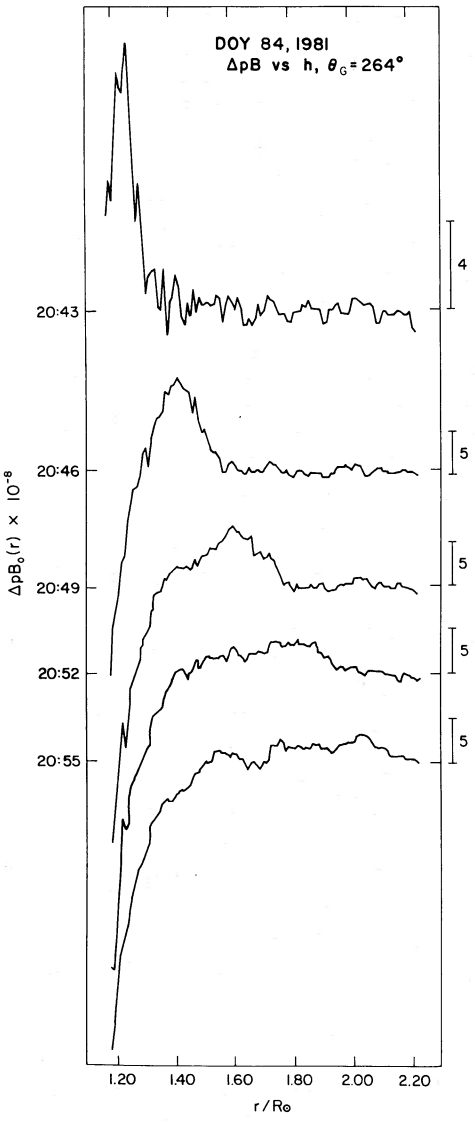

FIG. 3

diagnostic for the leading edge and the point of maximum polarization brightness for this event. The results are presented in Table 1 and height-versus-time diagram for ΔpB_{max} is shown in Figure 4. The sense of the scan was such that the azimuth $\Theta_G = 264°$ was reached 21.9 s after the time logged for the start of the scan. In Figure 4, the points are joined by straight line segments between the data points, and it appears that there is a slight acceleration of the leading edge as a function of time. However, it must be recognized that, in fact, a single line segment with constant slope can pass through all the measurements within their estimated errors.

The apparent speed of the leading edge is more difficult to measure than the speed of ΔpB_{max} because of the presence of noise. The estimates for the speed of the leading edge are equal to those for ΔpB_{max} up to the uncertainty of measurement.

An attempt to understand the variation in coronal mass was made, even without a sophisticated knowledge of the

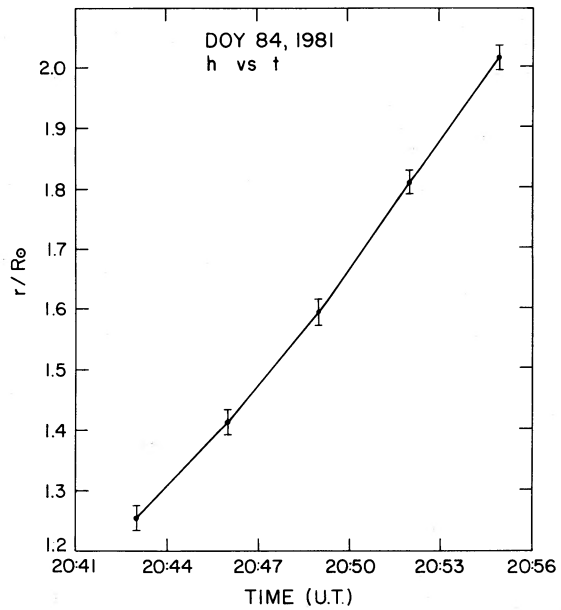

FIG. 4

FIG. 3—$\Delta pB(h)$ as a function of time. Note the scale change between 2043 and 2046 UT. The scale for each trace is set by a 4 or 5 × 10^{-8} pB mark in the right-hand side of the plot.

FIG. 4.—Temporal variation of the height of the leading edge of the 1981 March 25 transient. Note that the times given are image start times and that the scan aperture used for this analysis crosses $\Theta_G = 264°$ 21.9 s later than the indicated time.

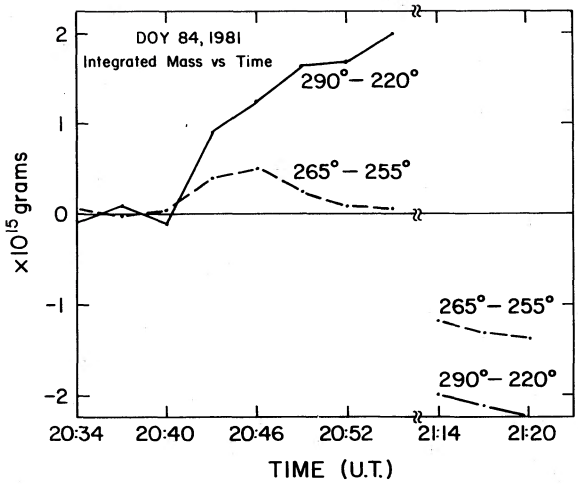

FIG. 5.—Integrated mass difference inferred from subtracted images using a base frame taken at 2034 UT. The nonzero values of the first points are attributed to noise in the subtraction process. For these estimates of mass, it is assumed that all coronal material observed is restricted to the plane of the sky.

distribution of coronal material along the line of sight. If it is assumed that all the variations observed in pB and ΔpB are restricted to the plane of the sky, it is then possible to scale the digital data and obtain an estimate of the mass per pixel or difference in mass per pixel. We have assumed a standard cross section for the Thomson scattering of photospheric radiation (Billings 1966), the van de Hulst (1950) formulation for the scattering by electrons illuminated by a limb-darked disk, and a coronal mass per electron of 2×10^{-24} g, equivalent to the assumption of 10% abundance of He by number following Hildner *et al.* (1975). With this approach, we have assigned a value of differential mass to each pixel in the ΔpB images and integrated over sectors of 10° in azimuth, in one case, and 70° in the other. These sectors are shown in Figure 2.

By assuming differential mass $\delta m(h, \theta, t)$ over height and sector, it is possible to characterize the approximate change in coronal mass, for both the central portion of the looplike structure (10° sector) and as well as the entire event (70° sector), as a function of time as a result of the transient's passage, i.e.,

$$\Delta M(t) = \int_{1.18\,R_\odot}^{2.36\,R_\odot} \int_{\Theta_1}^{\Theta_2} \delta m(h, \theta, t) h dh d\theta \,, \qquad (1)$$

where $\Delta M(t)$ is now defined as the total change in mass between a reference image and an image obtained at a later time for either the wide or narrow sector. The height variation of the change in mass requires only the integration over the azimuth, and this second quantity $\Delta M(h, t)$.

$$\Delta M(h, t) = \int_{\Theta_1}^{\Theta_2} \delta m(h, \theta, t) h d\theta \,, \qquad (2)$$

refers to the fraction of mass change at a particular height h (a single diode) at a particular time t. Each diode samples a region in the corona which is 10.″6 in radial extent. The time variation of the first quantity, namely the change in the total coronal mass as a function of time—assuming that all material is restricted to the plane of the sky—is shown in Figure 5 for both the 10° sector and the 70° sector. In this diagram, a break in the data stream is shown in the plot starting at 2055 UT and lasting until 2114 UT. This is an artifact generated by the need to halt observations in order to reposition the dome. The leading edge of the transient was beyond the limit of the field of view in the partial raster started at 2058 UT, so the maximum integrated value observable for the entire event structure was detected in the trace marked 290°–220° (70° sector, *solid line*) at 2055 UT.

This graph serves to illustrate several points concerning the integrated mass changes observed. First, at least 2×10^{15} g was injected into the field of view from beneath the occulting disk; the mass depleted from the lower corona was not simply repositioned to make a density enhancement higher in the corona. That is, ΔM(2055 UT) is positive, and this fact eliminates the possibility that the appearance of the ΔpB image represents only the consquence of rearrangment of material within the instrument's field of view. Second, there is a net depletion of the lower corona observed after the event, and the magnitude of this depletion is approximately 2.2×10^{-15} g. From these two mass estimates, we infer that at least half of the *total* mass change in the lower corona was the result of mass flow upward from a region lower than 1.18 $R_\odot$, as evidenced by conditions prior to 2055 UT, and that the other half of the total change in the mass within the field of view was the result of removing previously existing coronal structures. Third, it is possible to understand something about the distribution of mass by comparison of the data from both sectors. Within the 10° sector the development of the depleted region behind the bright archlike structure almost exactly balances the initial injection of mass into the field of view. The 70° sector encompasses a region of the coronal image which is considerably larger than the entire transient event, while the 10° central sector roughly includes both the leading edge and the depletion behind the leading edge. The initial increase of mass in the 10° sector is only about one-quarter of the increase detected in the 70° sector at 2055 UT, and this implies that much of the material which is added to the entire field of view at that time resides within the legs of the transient. Fourth, the trend observed at the right of Figure 5, namely continued depletion as time increases, is greater than the noise level of the instrument and is taken to be significant. Sky transmission records, independently measured in the Mk III bandpass, show no indication of variation of atmospheric transparency, and thus it is concluded that material was, in fact, still being removed from the lower corona from a volume near the azimuth $\Theta_G = 264°$ late in the event. Finally, since we have restricted the change in material to be strictly in the plane of the sky, the magnitudes inferred for the mass changes are lower limits to both enhancements and depletions (The efficiency of scattering is only lowered as one considers coronal structures removed from the plane of the sky.) This plane of the sky mass model will prove useful in the later comparison of a specific transient structure model with these inferred mass changes.

II. MODEL TRANSIENT EVENT, 1981 MARCH 25

We shall now construct an empirical model, attempting to account for the observed pB distribution of the transient by postulating three-dimensional configurations for the production of electron scattering of photospheric radiation. Having

specified electron density models, which are necessarily required to match the observed spatial distribution of $pB(h)$, we will specifically test the assumption of restricting the transient to the plane of the sky. This assumption was used to estimate the change in mass properties in the previous section without resorting to three-dimensional models. These steps were taken with the intent of gaining insight into the geometrical properties of the transient structure and understanding of coronal mass changes through the lifetime of the event.

For three-dimensional model construction, the first simplification made is that the radial gradient in the electron density, $N_e(r)$ is everywhere governed by the Saito (1970) power-law formulation, namely

$$N_e(r) = \bar{N}(C_1 r^{-2.5} + C_2 r^{-6} + C_3 r^{-16}), \quad (3)$$

where $\bar{N}$ is an arbitrary multiplier chosen to match the observed pB signal, and $C_1 = 2.5 \times 10^{+6}$, $C_2 = 1.58 \times 10^{+8}$, and $C_3 = 3.10 \times 10^{+8}$ and r is measured in solar radii. From previous experience with fitting observed pB distributions, it is expected that this power law will yield satisfactory results. Two further assumptions are required before calculations can be made. We shall use Minnaert's (1930) formulation for estimation of the components of partially polarized light scattered from coronal electrons. This provides a means for estimating any of the observable quantities of the white light corona, brightness, B, polarized brightness, pB, and polarization, p, once a distribution of electron density is defined. In this case we deal only with the product of the polarization of the white light corona and the coronal brightness, because this is the only quantity that the K-coronameter is capable of measuring. For an arbitrary electron density model $N_e(r)$ observed at a height h in the plane of the sky, $pB(h)$ and $B(h)$ are estimated from the quantities

$$I_t - I_r = pB(h) = \frac{B_\odot \pi\sigma}{2[1 - (u/3)]} \int_{-\infty}^{+\infty} N_e(r)\left(\frac{h}{r}\right)^2 [(1-u)A + uB]ds \quad (4)$$

$$I_t(h) = \frac{B_\odot \pi\sigma}{2[1 - (u/3)]} \int_{-\infty}^{+\infty} N_e(r)[(1-u)C + uD]ds, \quad (5)$$

where $B(h) = I_t + I_r$, σ is 7.95×10^{-26} sr^{-1}, u is an empirical function of effective wavelength (0.4 for the Mk III with its effective λ of 8200 Å), h is the height in the plane of the sky, r is the distance along the radius vector from the Sun to the point in question along the path of integration, ds, and A, B, C, and D are the Minnaert (1930) polarization parameters dependent upon r.

Using the above two equations, it is possible to investigate quantitatively the scattering properties of an assumed distribution $N_e(r)$. We will use the system $N_e(x, y, s)$ for $N_e(r)$, where x and y are coordinates within the plane of the sky parallel and perpendicular to the solar rotation axis and s is the third Cartesian coordinate perpendicular to x and y. However, to provide the reader with an appreciation for how the efficiency of scattering changes as a function of distance from the plane of the sky, we shall first examine a single height $h = 1.45\ R_\odot$. In Figure 6, the normalized efficiency of scattering, $B = I_t + I_r$, is plotted as a function of phase angle, Θ, the angle between a radius vector from the center of the Sun to a point P somewhere along the line of sight at height $h = 1.45\ R_\odot$ and the vector in the plane of the sky which intersects the line of sight. $\Theta = 0°$ for a point in the plane of the sky. The percent polarization of the white light corona, p, is also shown on this same graph along with the polarized brightness, pB, the product of these previous two quantities. Two points illustrated by Figure 6 are useful in the context of the analysis of white light transients. The portion of the line of sight that is well observed by a K-coronameter technique is significantly shorter than an equivalent observation by a coronagraph which also observes the quantity B (such as an externally occulted orbiting coronagraph). The relative efficiencies of the scattering processes for B and pB fall to their respective half-power values at phase angles of 51° and 36°, respectively. For structures embedded in the corona at a reference height of 1.45 $R_\odot$, the integration path length has the scale of $S = 1.45\ R_\odot \tan\Theta$, or distances 1.79 and 1.05 $R_\odot$ for B and pB, respectively. From this analysis, it is seen that the volume of the corona observable with the K-coronameter technique is restricted to a region closer to the plane of the sky than, for example, a white light eclipse observation. Second, for structures located within one-half of a radius from the plane of the sky, $\Theta = \pm 19°$ for $h = 1.45\ R_\odot$, the efficiency of scattering in pB does not vary rapidly, and it is possible to approximate the mass changes near the limb in the low corona with the assumption that all material is restricted to the plane of the sky. If this procedure is utilized, lower limits to both observed density depletions and enhancements are obtained. The scattering efficiency can only be lower if the material is located at a phase angle significantly larger than $\sim \pm 20°$—implying that greater densities are required to produce the observed effects.

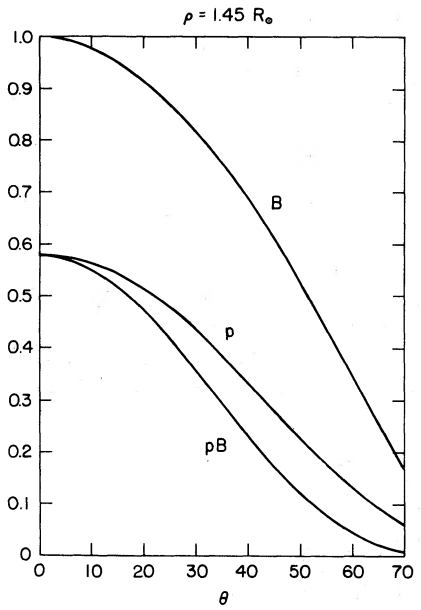

FIG. 6.—Relative efficiency of scattering at $h = 1.45\ R_\odot$. Plotted are the relative efficiency of scattering per electron, B, as a function of phase angle Θ (the angle between a radius vector from the center of the Sun to a point in the corona and the line of sight) as well as the variation of polarization, p, and the relative polarized brightness pB, the product of p and B.

The most striking feature seen in the difference contour,

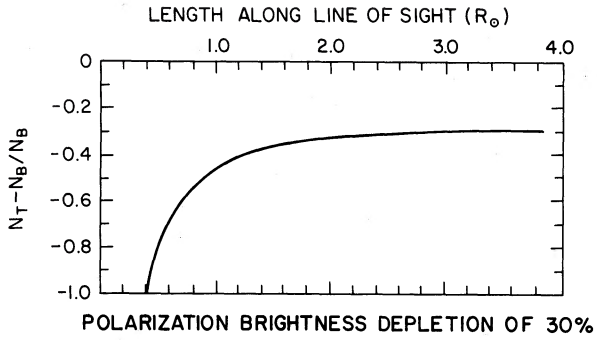

FIG. 7.—Relative observed depletion as a function of transient path length and a reduction of density for a 30% depletion in pB occurring at $h = 1.45\ R_\odot$.

Figure 1, is the depleted region created by the transient's passage through the lower corona. While the structure of enhanced region cannot be uniquely modeled, it is possible to use the depleted region to investigate the minimum physical dimension along the line of sight of coronal material that interacted with the transient. A tool for investigating this physical dimension is shown in Figure 7. This diagram relates the relative density of the depleted region, $(N_t - N_B)/N_B$, where N_t and N_B are the transient and background densities, to the path length along the line of sight through the transient required to produce a 30% reduction in the pB signal. The depleted area is taken to be symmetrically placed about the plane of the sky, and the coronal density model used is given by equation (3). If the depleted volume is taken to be a perfect vacuum, that is if $(N_t - N_B)/N_B = -1.0$, then the path length required to produce the observed depletion is about 0.4 $R_\odot$ along the line of sight. Because the active region associated with the transient being considered was located at W89, it is reasonable to assume that the transient occurred in a volume of corona near the plane of the sky. Because the observed depletion at the base of the transient, as seen at 2055 UT, is of the order of 30% in pB, by using the information developed above we are led to the conclusion that the *minimum* path length required to produce the observed effect is 0.4 $R_\odot$ for this case where spherical symmetry is assumed, if *all* coronal material previously existing prior to the transient is completely removed. The inferred path length can be much longer, of course, if only a fraction of the preexisting material was removed from the depleted volume.

We now turn to the specific model required to investigate the 1981 March 25 transient. A so-called ice cream cone model is used for three separate instances with different densities allocated for the cases of (*a*) the background corona as seen prior to the trainsient event, (*b*) the transient event as detected at 2055 UT, and (*c*) the posttransient corona as observed at 2114 UT. This "ice cream cone" (IC^2) model is shown schematically in Figure 8. The lower outer portion is identified with the straight legs (sides) of the transient. This is the cone portion of the model with its apex coinciding with the center of the Sun. The inner volume is contained by the legs and is capped by half of an ellipsoid centered at some height d from Sun center. The shell or top portion (the ice cream part) has an outer ellipsoidal boundary with the same center as its inner one for simplicity. The parameters fixing the shape of the ellipsoids are a and a' (in the radial direction), b and b' (in the plane of the observations), and c and c' (along the line of sight). The density can be specified separately in the background surrounding the transient, the legs, the top or shell, and the interior. The number of parameters may appear at first to be excessive, but most can be directly specified from geometrical measurements of the transient images themselves (i.e., a, a', b, b', d). Only the densities and the dimensions along the line of sight (c's) depend upon the assumed three-dimensional distribution of pB.

The goal is to create a model of $N_e(x, y, s)$ for the gross properties of the transient, perhaps ignoring some of the fine structure and detail of the event, to infer its three dimensional geometry. For example by setting the value of the c parameter to a small value of the order of the difference $a' - a$ or $b' - b$ (the apparent width of the leading bright material or legs, respectively), it is possible to investigate numerically the scattering properties of a crude two-dimensional loop model. If the path length c is increased along the line of sight, s, one obtains a "bubble" or "bottle" model of a transient that is more three-dimensional in nature. We have demonstrated that the c dimension for the depleted region beneath the bright leading edge of this transient must be at least comparable in size to dimension in b.

The coronal density surrounding the entire region affected by the transient is successfully reproduced with a spherically symmetric density model whose magnitude, $\bar{N}$, is 1.35 times

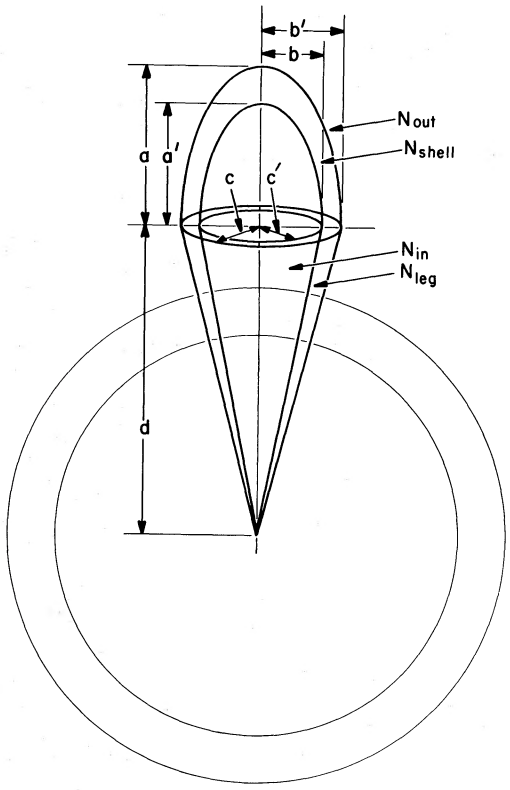

FIG. 8.—The schematic of the "ice cream cone" model depicting the various geometric parameters used in the specification of the coronal transient model.

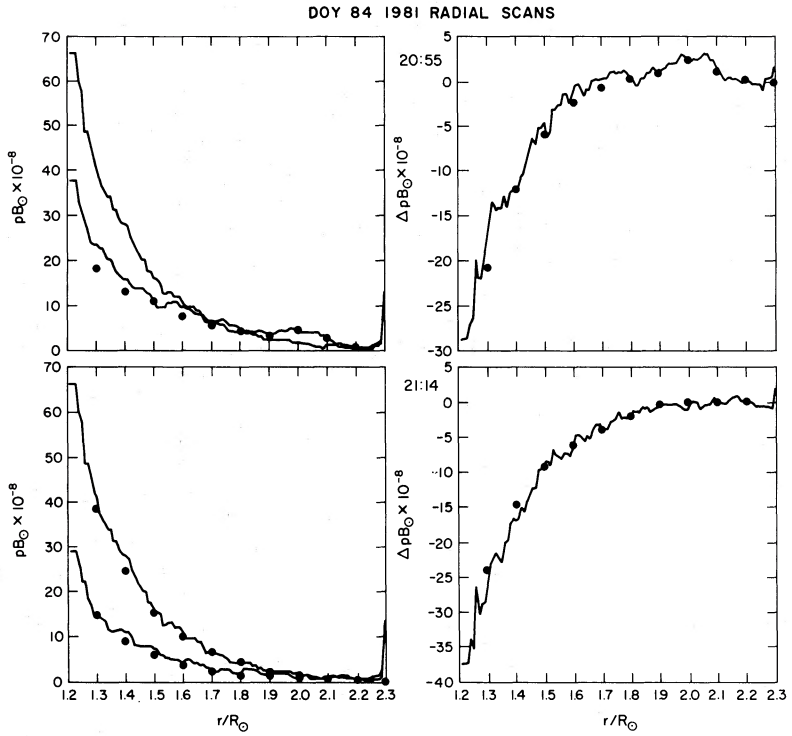

FIG. 9.—Radial scans of the corona, both $pB(h)$ (*left column*) and $\Delta pB(h)$ (*right column*) are shown for two times, 2055 (*top row*) and 2114 UT (*bottom row*). Data are indicated as solid lines; estimates of $pB(h)$ and $\Delta pB(h)$ obtained from the ice cream cone model are plotted with solid dots.

that of the Saito (1970) minimum quiet Sun density distribution. This value does not change for any of the three specific cases we have modeled: the pretransient corona, the transient event itself, and the post-transient corona. The discussion of these models is presented in order of increasing complexity. Line-of-sight information derived from the postevent model is required to specify the pretransient model.

Post-transient model (2114 UT).—To evaluate the minimum depth of the depletion as a function of height, the density of the depletion is set to zero. The observed radial variation of pB values through the center of the transient (shown in Fig. 9) is matched by a linear increase in the minimum depth as a function of height implying the coronal deficit has a wedge shape. It is deduced that $c = 0.2\ R_\odot$ at a height of $1.5\ R_\odot$. To extend this model to three dimensions, five azimuthal scans from 1.3 to $1.9\ R_\odot$ are used to deduce that the cone-shaped depletion has a width to depth ratio of approximately 3:2, and a leg density of a factor of 2 above the background (2.7 times the Saito model). A comparison of the model and the observation is depicted in Figure 10. If there is actually a finite density in the interior, then the depletion is even more extended along the line of sight (greater than $0.4\ R_\odot$ at a height of $1.5\ R_\odot$).

Pretransient model (2037 UT).—Because there was a pre-existing bright structure in the corona overlying the active region before the flare and resulting transient, the model is adjusted to resemble a streamer through the following modifications. First, we ignore the legs (i.e., set the density $N_{\rm leg}$ equal to the background density $N_{\rm out}$). To model the top, we also ignore the shell (set the density $N_{\rm shell}$ equal to the background). The shape of the top is best fitted by setting $d = 1.5\ R_\odot$ from Sun center, and $a = 0.5\ R_\odot$—making the total height of the "helmet" portion of the bright structure extend out to $2\ R_\odot$. The data in the outer field of view of the Mk III (2.0–2.2 $R_\odot$) are noisy and do not warrant extensive modeling of the bright feature above $2\ R_\odot$. Assuming the same depth c along the line of sight as determined for the void, a streamer density 5 times the Saito model is required to match the observations of the preevent image.

Coronal transient model (2055 UT).—We have selected the last frame which exhibited all features of the transient within the Mk III field of view. Again the interior density $N_{\rm in}$ is set to zero to place a lower limit on the thickness of the transient. The determination of the parameters a, a', b, b' for the top of the loop and the legs is accomplished by geometrical measurements of the apparent shape. The resulting model which best matches most of the observations has a leg density 4 times the Saito model and a shell, or top loop density, 15 times the Saito model. The thicknesses c and c' along the line of sight are identical to those determined for the postevent image—implying that the coronal volume affected by the transient did not significantly change once the depletion was formed.

III. COMPARISON OF MODELS WITH OBSERVATIONS

A summary of the physical distances derived for the three models, as well as the appropriate densities for various regions, is given in Table 2. In fitting numerical results to the observed pB distributions, sections along the radius oriented at 264° geocentric and azimuthal sections at fixed heights of 1.30, 1.60, and $1.90\ R_\odot$ were used. We have assumed that at 2055 and 2114 UT, the electron density in the depleted region is equal to zero, and we have adjusted c so that the observed value

of pB at $h = 1.30\ R_\odot$ is obtained. Using the other estimates for d, a, a', b, b', and setting $c - c' = b - b'$, it is then possible to estimate $pB(h, 2055)$ and $pB(h, 2114)$ as well as the radial differences $pB(h, 2055) - pB(h, 2037)$ and $pB(h, 2114) - pB(h, 2037)$. The observed data and the estimated radial distributions of $pB(h, t)$ and $\Delta pB(h, t)$ are shown in Figure 9. Observed quantities are displayed as a solid line while the radial variations of pB and ΔpB are indicated with heavy dots.

Azimuthal scans at heights above the limb, and the estimated azimuthal variations in $pB(h, \Theta)$ and $\Delta pB(h, \Theta)$ are shown in the nine panels of Figure 10. In the left-hand column the azimuthal variation of $pB(h, \Theta)$ is shown so that the reader is able to discern the existence of the preevent enhanced region at approximately the same azimuth as the subsequent transient. Differences, indicated to the right of this first column of graphs, show the major features of the transient: legs, depleted region, and enhanced leading edge. With the addition of a parameter for the density of the leg, the model estimates are relatively successful, at least in a quantitative sense, in recapitulating the major features depicted in the difference images (Fig. 2). We

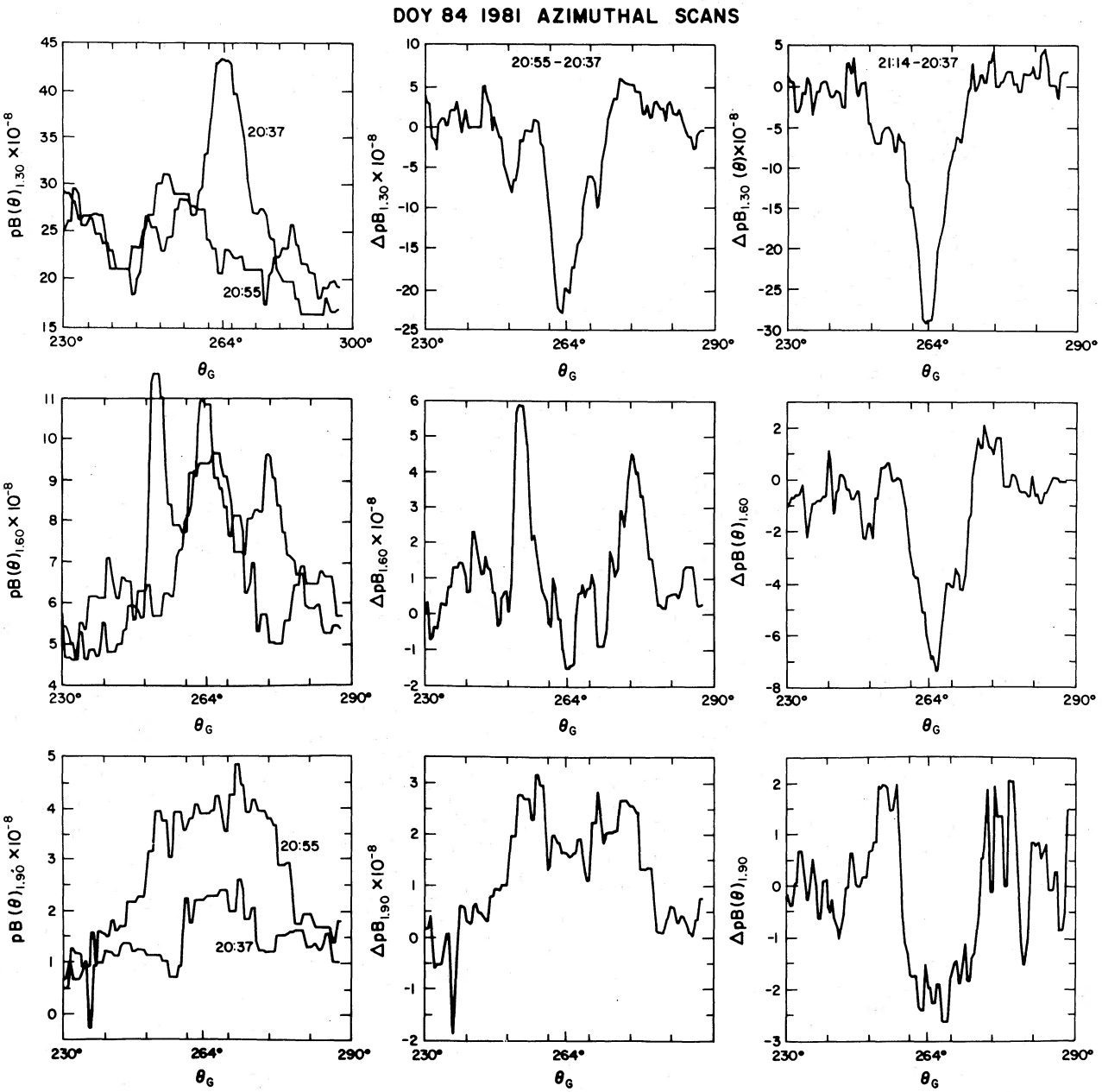

FIG. 10.—Observed azimuthal scans of pB and ΔpB. Rows in this plot refer to data and calculations at constant heights of 1.3 $R_\odot$ (*top row*), 1.6 $R_\odot$ (*middle row*), and 1.9 $R_\odot$ (*bottom row*). The heights of the azimuthal scans are indicated on Fig. 2. All plots in the left column show pB data taken before the transient (2037 UT) and during the transient event (2055 UT). The second column indicates the difference observed between 2037 and 2055 UT, while the right hand column shows the ΔpB distribution observed after the transient was beyond the field of view of the Mk III instrument.

TABLE 2

MODEL PARAMETERS FOR 1981 MARCH 25 TRANSIENT

Parameter	Pre	During	Post
Interior Density	5.0	0.0	0.0
Leg Density	...	4.0	2.7
Shell (top) Density	...	15.0	...
Background Density	1.35	1.35	1.35
Height (d)	1.50	1.50	∞
Inner a	0.50	0.50	...
Inner b (width)	0.30	0.30	0.30*
Inner c (los)	0.21	0.21	0.21*
Outer a'	...	0.80	...
Outer b' (width)	...	0.34	0.34*
Outer c' (los)	...	0.26	0.26*

NOTES.—Density values measured in multiples of Saito Quiet Background. Lengths measured in solar radii. Values marked with an asterisk for the posttransient model refer to distances at a height of 1.5 $R_\odot$.

do not intend to infer detailed physical parameters by the use of this transient model but rather are simply attempting to create a model which is necessary (in the mathematical sense) for fitting the observed data. Not all of the observed structure is accounted for by the present description; however, a transient structure that has a depth equivalent to the observed width in the plane of the sky is required to reproduce the major observed structures.

If the model density distributions do represent the gross characteristics of the observations, then for consistency the mass calculated from the model should mimic that previously inferred from the observations. For the three models derived above, the total mass at a given time was calculated via

$$M(t) = \int_{R_1}^{R_2} \int_{\Theta_1}^{\Theta_2} \int_{-\infty}^{+\infty} M_e N_e(\mathbf{r}) ds d\Theta h dh , \qquad (6)$$

where $N_e(\mathbf{r})$ is the electron density at a point P, h is height above the limb at an azimuth Θ defining a line of sight, s, and M_e is the mass per electron. These values are displayed (*open circles*) as differences in mass $\Delta M(t - 2034\ \mathrm{UT})$ for azimuthal segments of height 0.1 $R_\odot$ in Figure 11 for the same sectors of 10° and 70° width that were used for the plane of the sky estimates of the total mass change. Because we have insisted on a consistency in the calculated $pB(h, \Theta)$ and the observed pB distribution, the mass calculated from the models follow the inferred differential mass curves estimated from the observations. The total mass of depleted regions estimated from the model will generally be lower (enhanced mass regions higher) than estimates of differential mass obtained from observed pB values which are treated as if all matter were placed in the plane of the sky. This is a consequence of the physics of scattering of photospheric photons by electrons as shown in Figure 6 since the volume elements used in the model calculations are *not* restricted to the plane of the sky.

IV. DISCUSSION AND SUMMARY

By fitting a particular three-dimensional model to an observed change in the ΔpB field, the depleted regions of this coronal transient have been shown to have a depth along the line of sight which is similar to the dimension of the event as seen in the plane of the sky. In the latter stages of development, specifically at 2055 UT, some 14 minutes after the onset of the Hα flare associated with the transient, the depth of the depleted regions normal to the plane of the sky equaled or exceeded 0.5 $R_\odot$. This finding is a result of calculations which place a region of complete vacuum in the plane of the sky and then adjust the depth along the line of sight for this depleted volume until the observed difference in the polarized brightness of the corona is obtained. Because scattering efficiency is maximum at the plane of the sky, this assumption establishes only a lower limit for the amount of mass removed from the corona. Depletions located away from the plane of the sky will require even longer scale lengths to account for the observed decrease in pB. Similarly, assuming a complete void (zero density) independently establishes lower limits to extents along the line of sight; finite densities require greater extents. Estimates for the distribution of material in enhanced portions of the corona depend specifically upon the integral over the line of sight of a kernel function which varies linearly with electron density. While the models do reproduce the observed brightness distributions, they do not represent unique solutions. If the geometrical model is, in fact, valid for the enhanced regions as well as the depleted regions, and further, if a relatively simple power law may be employed for a height variation in N_e, then it is possible to infer some density characteristics of the transient.

A spherically symmetric corona with a radial variation as specified by the Saito solar minimum model but with an enhancement factor of $\bar{N} = 1.35$ is sufficient to represent the preexisting background distribution of pB. The flare-associated transient occurred at the same azimuth in the plane of the sky as a bright, radially oriented feature. This feature is easily modeled by embedding a structure with the same volume as the postevent model dimensions within the spherically symmetric component and enhancing the electron density by a factor of 3.7 over the background (a factor of 5 times the original Saito model). The specific model required for fitting the observed pB data fixes the density of the top portion of the transient at a value 15 times the Saito density model, an enhancement of a factor of 3 over the preexisting streamer density. Behind the enhanced shell it is assumed that the electron density is equal to zero, and the region has a dimension along the line of sight of 0.5 $R_\odot$ at a height of 1.5 $R_\odot$. The legs of the transient are not accurately modeled with the same factor of enhancement required for the leading edge. From other images of the event as it passed through the K-coronameter's field of view, the legs appear to be very dynamic (i.e., the pB signal is variable).

Integration of the density model over the 10° and 70° sectors and the line of sight suggest that results (Fig. 11) obtained are not grossly different from those inferred by simply putting all the transient mass (or deficit) into the plane of the sky. The mass change deduced from scaling the observed data (integrated over the 10° and 70° sectors) can be used to characterize the transient with a fair degree of accuracy. A mass of 2.0×10^{15} g of material was observed rising from behind the occulting disk as the first indication of the coronal transient. The lower corona was depleted following this initial injection and at the time the transient left the field of view, the amount of material removed from the preexisting corona in the 10° sector equaled the mass of material injected into this sector. The postevent ΔpB images suggest that at least

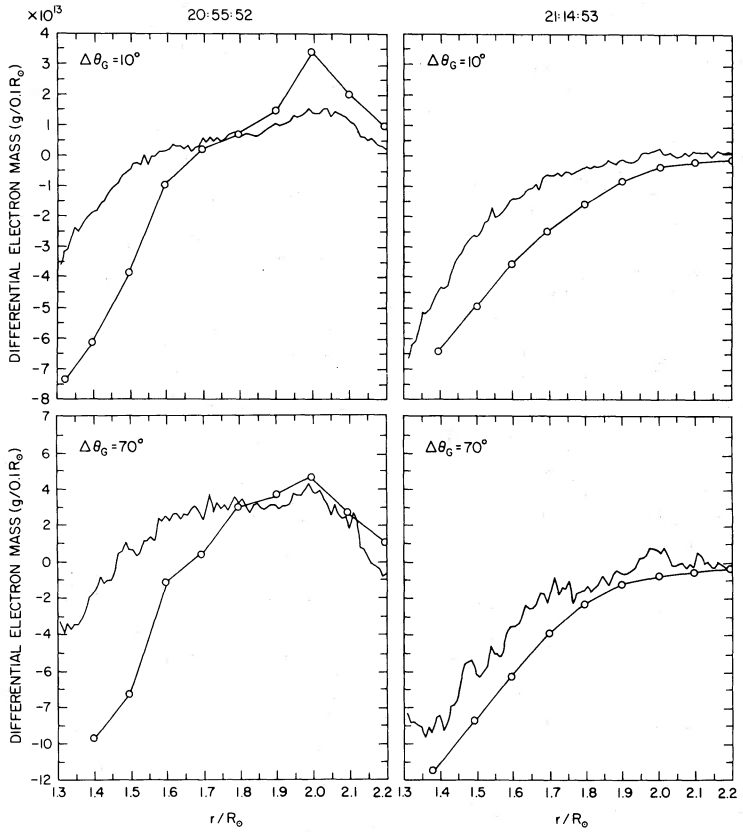

FIG. 11.—Distribution of differential mass as a function of height for the transient (2055 UT, *left column*) and posttransient depletion (2114 UT, *right column*). Mass estimates are plotted using the continuous solid line, assuming the coronal material observed is restricted to the plane of the sky. Mass estimates, obtained by and subtracting the preevent model from the ice cream cone and pastevent three-dimensional models of the distribution of coronal mass, are plotted with the line interrupted by open circles. Azimuthal integrations over sectors of 10° (*top row*) and 70° (*bottom row*) are shown for the two times. Since estimates obtained from the data depend upon the assumption of material restricted to the plane of the sky, enhanced regions tend to be underestimates for the differential mass, while estimates for the depleted regions tend to be overestimates when compared to the values of differential mass obtained from the three-dimensional models.

2.2×10^{15} g of material was removed from the corona with respect to pre-event coronal structures and that material was being slowly removed from this region even as late as 2120 UT (when the leading edge, if moving in the plane of the sky at a velocity of $\sim$800 km s^{-1}, would have been at a height of 3.7 $R_\odot$ above the limb). By using this simple analysis of mass to set lower limits, we find that (*a*) the net mass change of the lower corona was not less than 4.2×10^{15} g between the heights of 1.2 $R_\odot$ and about 2.34 $R_\odot$ as a result of the transient, and (*b*) about half of this material can be accounted for by the removal of preexisting coronal structures. The remaining material was injected from a region below the occulting disk. During the time that the entire transient structure was within the field of view, the difference image analysis shows that more mass was added to the lower corona from below the occulting disk than was depleted. It is *not* possible to account for the enhanced density in the leading edge by simply rearranging mass within the field of view.

In summary, the event described here appears similar in the lower corona to those flare-associated events seen with externally occulted orbiting coronographs which generally have viewed coronal heights greater than the HAO Mk III *K*-coronameter. A typical event for comparison—having similar radio and X-ray properties—occurred on 1974 January 17 and was described by Munro *et al.* (1977) from data collected with the S-052 instrument included in the ATM-*Skylab* experiment. Estimates of speed and mass have similar values for these two events; the morphology of both events is characterized as being "archlike." Thus it is concluded that the transient which occurred on 1981 March 25 was similar to previously observed flare-associated transients, and that the physical process which drove the transient originated at a height below the inner limit of the Mk III field of view (1.20 $R_\odot$). It is also concluded that about one-half of the total mass of the event came from the preexisting corona lower, $h < 2.34\ R_\odot$.

A new conclusion of this study is that the empirical model transient required to match the observations demands that the depleted portions of the transient must be approximately equal in depth, normal to the plane of the sky, to the characteristic dimensions seen in the plane of the sky. A consistent model, which has rotational symmetry about a radial axis normal to the limb, is the so-called ice cream cone model which has a core depleted to zero density.

This model is at considerable variance to the planar loop models adopted by Mouschovias and Poland (1978), Anzer

(1978), and Pneuman (1982). A hypothesis which resolves this apparent conflict is that flare-associated transients are, in fact, three-dimensional structures generated by the impulsive deposition of energy into the lower corona, and that true two-dimensional arches are generated in the solar corona by an entirely different physical mechanism. Further investigation of this hypothesis employing observations of other coronal transients will be the subject of a future study.

The High Altitude Observatory, a division of the National Center for Atmospheric Research, is sponsored by the National Science Foundation. The observations for this work were collected by C. Garcia and K. Rock of the Mauna Loa Solar Observatory. M. McCabe kindly provided Hα filtergram of the disk and limb from the Mees Solar Observatory, Institute for Astronomy, Haleakala, Maui, Hawaii. D. Friend provided data reduction assistance for the variation of mass study. The authors wish to express their gratitude to R. Stewart of C.S.I.R.O., for providing information concerning the radio emission of this event and T. Holzer and E. Hildner who carefully read the manuscript and made several helpful suggestions.

REFERENCES

Anzer, U. 1978, *Solar Phys.*, **57**, 111.
Billings, D. E. 1966, *A Guide to the Solar Corona* (New York: Academic Press), pp. 152–153.
Fisher, R. R., and Poland, A. I. 1981, *Ap. J.*, **246**, 1004.
Friend, D., Munro, R. H., Fisher, R. R., and McCabe, M. K. 1982, *Bull. AAS*, **13**, 890.
Hildner, E., Gosling, J. T., MacQueen, R. M., Munro, R. H., Poland, A. I., and Ross, C. L. 1975, *Solar Phys.*, **42**, 163.
McCabe, M. K. 1981, private communication.
Minnaert, M. 1930, *Zs. Ap.*, **1**, 209.
Mouschovias, T. Ch., and Poland, A. I. 1978, *Ap. J.*, **220**, 675.
Munro, R. H., Gosling, J. T., Hildner, E., MacQueen, R. M., Poland, A. I., and Ross, C. L. 1979, *Solar Phys.*, **61**, 201.
Pneuman, G. 1980, *Solar Phys.*, **65**, 369.
Rock, K., and Seagraves, P. 1982, NCAR Technical Note NCAR/TN-200+IA.
Saito, K. 1970, *Ann. Tokyo Astr. Obs., 2d series*, **12**, 53.
Solar-Geophysical Data 1981, No. 440, Part I, p. 25 (Boulder: NOAA).
Stewart, R. 1981, private communication.
van de Hulst, H. C. 1950, *Bull. Asdr. Inst. Netherlands*, **11**, 135.

RICHARD FISHER and RICHARD MUNRO: High Altitude Observatory, P.O. Box 3000 Boulder, CO 80307